Research Article | Vol. 26, No. 25 | 10 Dec 2018 | OPTICS EXPRESS 32918
Optics EXPRESS

Asymmetric light diffraction of two-dimensional electromagnetically induced grating with *PT* symmetry in asymmetric double quantum wells

SI-CONG TIAN,[1,5] REN-GANG WAN,[2,5] LI-JIE WANG,[1] SHI-LI SHU,[1] HUNA-YU LU,[1,4] XIN ZHANG,[1,4] CUN-ZHU TONG,[1,*] JING-LIANG FENG,[3] MIN XIAO,[3] AND LI-JUN WANG[1]

[1]*State Key Laboratory of Luminescence and Applications, Changchun Institute of Optics, Fine Mechanics and Physics, Chinese Academy of Sciences, Changchun 130033, China*
[2]*School of Physics and Information Technology, Shaanxi Normal University, Xi'an 710062, China*
[3]*Department of Physics, University of Arkansas, Fayetteville, Arkansas 72701, USA*
[4]*The University of Chinese Academy of Sciences, Beijing 100049, China*
[5]*Si-Cong Tian and Ren-Gang Wan contributed equally to this work.*
**tongcz@ciomp.ac.cn*

Abstract: An asymmetric double semiconductor quantum well is proposed to realize two-dimensional parity-time (*PT*) symmetry and an electromagnetically induced grating. In such a nontrivial grating with *PT* symmetry, the incident probe photons can be diffracted to selected angles depending on the spatial relationship of the real and imaginary parts of the refractive index. Such results are due to the interference mechanism between the amplitude and phase of the grating and can be manipulated by the probe detuning, modulation amplitudes of the standing wave fields, and interaction length of the medium. Such a system may lead to new approaches of observing *PT*-symmetry-related phenomena and has potential applications in photoelectric devices requiring asymmetric light transport using semiconductor quantum wells.

1. Introduction

Electromagnetically induced transparency (EIT) [1–3] is one of the most typical phenomena based on laser-induced atomic coherence. EIT has important applications in several fields such as slow light [4,5], light storage [6,7], optical switching [8,9], enhanced Kerr nonlinearity [10,11], and four-wave mixing [12,13]. When a traveling wave (TW) field is replaced by a standing wave (SW) field in systems with EIT, the absorption and dispersion of the probe field will become spatially periodic, and photonic bandgaps [14,15] and electromagnetically induced gratings (EIGs) [16–20] can thus be formed. In EIGs, the amplitude and phase modulations of the transmission function can be flexibly modulated, and the intensity distribution of different orders of the grating can be manipulated. Therefore, EIGs have a number of potential applications in the field of optical switching and routing [21], optical solitons [22], and photonic Floquet topological insulators [23].

Similarly, the non-Hermitian parity-time (*PT*)-symmetric Hamiltonian, which was first proposed in 1998 [24], has attracted great attention, and it has been extended to optical systems [25] and observed experimentally [26,27]. In systems with *PT symmetry*, the profile of the real part of the refractive index is symmetric, while that of the imaginary part is antisymmetric, that is, $n(x) = n^*(-x)$. Because of this unique property, several interesting phenomena have been unveiled in systems with optical *PT symmetry*, including optical solitons [28], non-Hermitian Bloch oscillations [29], unidirectionally propagating photons [30–34], unidirectional diffraction [35–37], perfect absorbers [38,39], photons [40,41] lasers,

#342623 https://doi.org/10.1364/OE.26.032918
Journal © 2018 Received 23 Aug 2018; revised 8 Nov 2018; accepted 9 Nov 2018; published 3 Dec 2018

Optics EXPRESS

and phonon lasers [42,43]. In addition, *PT symmetry* has recently been theoretically [44–46] and experimentally [47] demonstrated in atomic systems.

In recent years, semiconductor quantum wells (QWs) have been investigated to realize quantum coherence and the interference effect [48–52]. Compared to atomic systems, semiconductor QW systems have designable and flexible of energy levels, and they are ease of integration and stable for practical application. Motivated by this research, in this study, we investigate the optical properties of asymmetric double semiconductor QWs driven by one TW probe field and two-dimensional (2D) SW coupling and pump fields. We show that in such a QW system, 2D *PT symmetry* and a nontrivial 2D EIG can be realized. The probe photons traveling through the QWs can be diffracted into the selected domain depending on the spatial relationship of the real and imaginary parts of the refractive index. We find that such asymmetric diffraction patterns in QWs can be controlled by the sign of the probe field and the modulation amplitudes of the 2D SW coupling and pump fields, and the intensity distribution in the selected domain can be manipulated by varying the interaction length of the QWs.

2. Models and equations

We consider asymmetric double semiconductor QWs [53], which consist of a 51-monolayer (145 Å)-thick wide well (WW) and 35-monolayer (100 Å)-thick narrow well (NW), between which there is a 9-monolayer (25-Å)-thick $Al_{0.2}Ga_{0.8}As$ barrier, as shown in Fig. 1(a). There are ten pairs of QWs (each pair consists of one WW, one NW, and one thick barrier), which are isolated from each other by 200-Å-wide $Al_{0.2}Ga_{0.8}As$ buffer layers. All these pairs are sandwiched between nominally undoped 3500-Å-thick $Al_{0.2}Ga_{0.8}As$ layers.

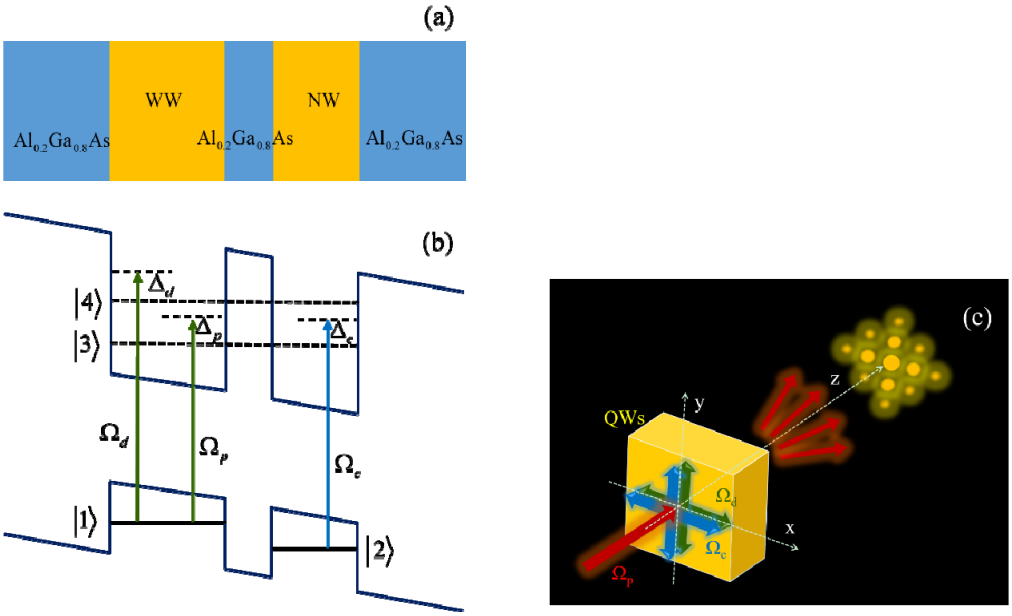

Fig. 1. (a) Schematic of one pair of asymmetric double QWs with buffer layers. (b) Band diagram of the asymmetric double QWs. (c) Geometry of laser beams applied to the asymmetric double QWs along the z-direction, and the corresponding far-field diffraction patterns of the probe field.

Such asymmetric double semiconductor QWs can be treated as a four-level N configuration [54–56], as shown in Fig. 1(b). Here, levels $|1\rangle$ and $|2\rangle$ are localized hole states in a valence band, while levels $|3\rangle$ and $|4\rangle$ are delocalized bonding and antibonding

Optics EXPRESS

states in a conduction band, respectively, arising from the tunneling effect between the WW and NW via the thin barrier. The probe field E_{p} with frequency ω_p probes the transition $|1\rangle \to |3\rangle$, while the coupling field E_{c} with frequency ω_c and the pump field E_{d} with frequency ω_d act on transitions $|2\rangle \to |3\rangle$ and $|1\rangle \to |4\rangle$, respectively. The Rabi frequency of the probe, coupling, and pump fields are $\Omega_p = \mu_{13}E_p/2\hbar$, $\Omega_c = \mu_{23}E_c/2\hbar$, and $\Omega_d = \mu_{14}E_d/2\hbar$, respectively, where μ_{ij} is the associated dipole transition matrix element, and the detuning of the probe, coupling, and pump fields are $\Delta_p = \omega_p - \omega_{31}$, $\Delta_c = \omega_c - \omega_{32}$, and $\Delta_d = \omega_d - \omega_{42}$, respectively, where ω_{ij} is the transition frequency between levels $|i\rangle$ and $|j\rangle$.

Under the condition of low QW carrier density, many-body effects due to electron–electron interactions can be neglected [57]. In the interaction picture and under the rotating wave approximation, the Hamiltonian of the QW system can be written as ($\hbar = 1$)

$$\begin{aligned} H = &\left(\Delta_c - \Delta_p\right)|2\rangle\langle 2| - \Delta_p|3\rangle\langle 3| - \Delta_d|4\rangle\langle 4| \\ &+\left[\Omega_p|1\rangle\langle 3| + \Omega_c|2\rangle\langle 3| + \Omega_d|1\rangle\langle 4| + \text{H.c.}\right]. \end{aligned} \tag{1}$$

Here, H.c. is the Hamiltonian complex conjugate.

The equation of motion for the density matrix of the system under the relaxation process is

$$\dot{\rho} = -i[H,\rho] - \frac{1}{2}\{\tilde{\gamma},\rho\}, \tag{2}$$

where $\tilde{\gamma}$ is the dissipation matrix. Substituting Eq. (1) into Eq. (2), the density matrix for each element can be obtained:

$$\dot{\rho}_{22} = i\Omega_c\left(\rho_{32} - \rho_{23}\right) + \Gamma_{42}\rho_{44} + \Gamma_{32}\rho_{33} - \Gamma_2\rho_{22}, \tag{3a}$$

$$\dot{\rho}_{33} = i\Omega_c\left(\rho_{23} - \rho_{32}\right) + i\Omega_p\left(\rho_{13} - \rho_{31}\right) - \Gamma_3\rho_{33} + \Gamma_{43}\rho_{44}, \tag{3b}$$

$$\dot{\rho}_{44} = i\Omega_d\left(\rho_{14} - \rho_{41}\right) - \Gamma_4\rho_{44}, \tag{3c}$$

$$\dot{\rho}_{12} = -i\Omega_c\rho_{13} + i\Omega_p\rho_{32} + i\Omega_d\rho_{42} - \tilde{\gamma}_{12}\rho_{12}, \tag{3d}$$

$$\dot{\rho}_{13} = -i\Omega_c\rho_{12} + i\Omega_d\rho_{43} + i\Omega_p\left(\rho_{33} - \rho_{11}\right) - \tilde{\gamma}_{13}\rho_{13}, \tag{3e}$$

$$\dot{\rho}_{14} = i\Omega_p\rho_{34} + i\Omega_d\left(\rho_{44} - \rho_{11}\right) - \tilde{\gamma}_{14}\rho_{14}, \tag{3f}$$

$$\dot{\rho}_{23} = -i\Omega_p\rho_{21} + i\Omega_c\left(\rho_{33} - \rho_{22}\right) - \tilde{\gamma}_{23}\rho_{23}, \tag{3g}$$

$$\dot{\rho}_{24} = -i\Omega_d\rho_{21} + i\Omega_c\rho_{34} - \tilde{\gamma}_{24}\rho_{24}, \tag{3h}$$

$$\dot{\rho}_{34} = i\Omega_p\rho_{14} - i\Omega_d\rho_{31} + i\Omega_c\rho_{24} - \tilde{\gamma}_{34}\rho_{34}, \tag{3i}$$

with $\rho_{11} + \rho_{22} + \rho_{33} + \rho_{44} = 1$ and $\rho_{ij} = \rho_{ji}^*$. Γ_{ij} is the natural decay rate between levels $|i\rangle$ and $|j\rangle$, and we assume that the decay rates from levels $|3\rangle$ and $|4\rangle$ in the conduction band to levels $|1\rangle$ and $|2\rangle$ in the valence band are identical. There is also no decay in the valence

Optics EXPRESS

band or conduction band, that is, $\Gamma_{31}=\Gamma_{32}$, $\Gamma_{41}=\Gamma_{42}$, and $\Gamma_{21}=\Gamma_{43}=0$, and $\Gamma_i=\sum_j^{i-1}\Gamma_{ij}$ denotes the total decay rate of level $|i\rangle$. We define $\tilde{\gamma}_{12}=\gamma_{12}+i\left(\Delta_p-\Delta_c\right)$, $\tilde{\gamma}_{13}=\gamma_{13}+i\Delta_p$, $\tilde{\gamma}_{14}=\gamma_{14}+i\Delta_d$, $\tilde{\gamma}_{23}=\gamma_{23}+i\Delta_c$, $\tilde{\gamma}_{24}=\gamma_{24}+i\left(\Delta_c+\Delta_d-\Delta_p\right)$, and $\tilde{\gamma}_{34}=\gamma_{34}+i\left(\Delta_d-\Delta_p\right)$, where $\gamma_{ij}=\left(\Gamma_i+\Gamma_j\right)/2$.

In such QW systems, $\Gamma_3=\Gamma_{3l}+\Gamma_3^{dph}$ and $\Gamma_4=\Gamma_{4l}+\Gamma_4^{dph}$, where Γ_{3l} and Γ_{4l} are the population decay rate of subbands $|3\rangle$ and $|4\rangle$, respectively, resulting from longitudinal-optical phonon emission events at low temperature, and Γ_3^{dph} and Γ_4^{dph} are the dephasing decay rates of quantum coherence due to electron-electron scattering, phonon scattering processes, and elastic interface roughness. For simplicity, we assume there is no interference or dephasing between levels $|3\rangle$ and $|4\rangle$, which can be realized based on the appropriate reduction of the temperature [52].

In the condition of $\Omega_p \ll \Omega_p, \Omega_d, \Gamma_3, \Gamma_4$, by solving Eq. (3), the first-order steady-state solution of $\rho_{31}^{(1)}$ can be obtained:

$$\rho_{31}^{(1)}=\frac{iA\left(\rho_{33}^{(0)}-\rho_{11}^{(0)}\right)+B\Omega_c\rho_{23}^{(0)}+C\Omega_d\rho_{14}^{(0)}}{A\tilde{\gamma}_{13}+B\Omega_c^2+C\Omega_d^2}\Omega_p, \tag{4}$$

where $A=\tilde{\gamma}_{12}\tilde{\gamma}_{24}\tilde{\gamma}_{34}+\tilde{\gamma}_{34}\Omega_d^2+\tilde{\gamma}_{12}\Omega_c^2$, $B=\tilde{\gamma}_{24}\tilde{\gamma}_{34}-\Omega_d^2+\Omega_c^2$, and $C=\tilde{\gamma}_{12}\tilde{\gamma}_{24}+\Omega_d^2-\Omega_c^2$. Because the separation between levels $|3\rangle$ and $|4\rangle$ is not large, the population decay rate of levels $|3\rangle$ and $|4\rangle$ can be equal ($\Gamma_{3l}=\Gamma_{4l}$), and dephasing decay rates of levels $|3\rangle$ and $|4\rangle$ can also be equal ($\Gamma_{3l}^{dph}=\Gamma_{4l}^{dph}$), which are reasonable and practical [54–56]. Therefore, the total decay rate of levels $|3\rangle$ and $|4\rangle$ can be the same ($\Gamma_3=\Gamma_4$), and thus $\gamma_{13}=\gamma_{23}=\gamma_{14}=\gamma_{24}=\gamma_{34}/2=\Gamma_3/2=\Gamma_4/2=\gamma$. Then, the zeroth-order terms in Eq. (4) can be obtained:

$$\rho_{33}^{(0)}=\frac{\Omega_c^2\Omega_d^2}{\Omega_d^2\left(2\Omega_c^2+\gamma^2+\Delta_c^2\right)+\Omega_c^2\left(2\Omega_d^2+\gamma^2+\Delta_d^2\right)}, \tag{5a}$$

$$\rho_{11}^{(0)}=\frac{\Omega_d^2+\gamma^2+\Delta_d^2}{\Omega_d^2}\rho_{33}^{(0)}, \tag{5b}$$

$$\rho_{23}^{(0)}=\frac{-i\gamma+\Delta_c}{\Omega_c}\rho_{33}^{(0)}, \tag{5c}$$

It should be noted that the condition of $\gamma_{13}=\gamma_{23}=\gamma_{14}=\gamma_{24}=\gamma_{34}/2=\Gamma_3/2=\Gamma_4/2=\gamma$ is not necessary for the following calculation. Without this condition, $\rho_{31}^{(1)}$ can also be calculated by Eq. (3), however, it is hardly to give the analytic solution.

Next, the susceptibility of the QW medium can be obtained through the following equation:

$$\chi=\frac{N\mu_{13}}{\varepsilon_0 E_p}\rho_{31}^{(1)}=\frac{N\mu_{13}^2}{2\varepsilon_0\hbar}\cdot\frac{\rho_{31}^{(1)}}{\Omega_p}, \tag{6}$$

where N is the electron density of the QWs and $\chi=\chi_R+i\chi_I$. χ_R describes the dispersion properties of the probe field, while χ_I describes the absorption properties of the probe field with $\chi_I>0\,(\chi_I<0)$ indicating loss (gain). To achieve *PT symmetry*, the refractive index n must satisfy the condition of $n(r) = n^*(r)$. The refractive index $n=\sqrt{1+\chi}=1+\chi/2$ and $n = n_0 + n_R + in_I$. Then, the real ($n_R=\chi_R/2$) and imaginary ($n_I=\chi_I/2$) parts of the refractive index can be obtained, with $n_0 = 1$ being the background index of the system. In the following calculations, for simplicity, we use the unit $N\mu_{13}^2/4\varepsilon_0\hbar$ for the refractive index.

Then, the interaction length of the QWs probed by the probe field along the z-direction is assumed to be L, of which the unit is $\zeta=\varepsilon_0\hbar\lambda\gamma/\pi N\mu_{13}^2$, and λ is the wavelength of the probe field. In the steady-state regime and under the slowly varying envelope approximation, Maxwell's equation of the probe field propagation is

$$\frac{\partial E_p}{\partial_z}=(-\alpha+i\beta)E_p, \tag{7}$$

where $\alpha=2\pi\chi_I/\lambda$ and $\beta=2\pi\chi_R/\lambda$. Then, the transmission function of the probe field for the interaction length L of the QWs modulated in both the x and y-directions can be given by

$$T(x,y)=e^{-\alpha L}e^{i\beta L}, \tag{8}$$

where $e^{-\alpha L}$ and $e^{i\beta L}$ represent the amplitude and phase component, respectively.

To achieve normal 2D EIG with symmetric diffraction patterns, only the pump field needs to be periodically modulated by the method of 2D SW fields in the x- and y- directions [58]. However, our goal here is to achieve a 2D EIG with asymmetric diffraction patterns, so the coupling field must also be periodically modulated, as shown in Fig. 1(c). Therefore, the coupling and pump fields can be written as

$$\begin{aligned}\Omega_c&=\Omega_{c0}+\delta\Omega_{cx}\cos\left[2\pi(x-x_i)/\Lambda_x\right]+\delta\Omega_{cy}\cos\left[2\pi(y-y_i)/\Lambda_y\right],\\ \Omega_d&=\Omega_{d0}+\delta\Omega_{dx}\sin\left[2\pi(x-x_i)/\Lambda_x\right]+\delta\Omega_{dy}\sin\left[2\pi(y-y_i)/\Lambda_y\right],\end{aligned} \tag{9}$$

where $\Lambda_x\,(\Lambda_y)$ is the space period of the SW coupling (pump) field and can be adjusted in a large range by tuning the angle between each component of the coupling (pump) field. $\Omega_{c0}\,(\Omega_{d0})$ is the initial amplitude of the SW coupling (pump) field, and $\delta\Omega_{cx}$ and $\delta\Omega_{cy}$ ($\delta\Omega_{dx}$ and $\delta\Omega_{dy}$) are the modulation amplitudes of the SW coupling (pump) field.

Considering that the probe field is a plane wave, the Fourier transformation of $T(x, y)$ yields the far-field intensity or Fraunhofer diffraction equation [16]:

$$I(\theta)=\left|E_p(\theta)\right|^2\frac{\sin^2\left(M_x\pi\Lambda_x\sin\theta_x/\lambda\right)}{M_x^2\sin^2\left(\pi\Lambda_x\sin\theta_x/\lambda\right)}\cdot\frac{\sin^2\left(M_y\pi\Lambda_y\sin\theta_y/\lambda\right)}{M_y^2\sin^2\left(\pi\Lambda_y\sin\theta_y/\lambda\right)}, \tag{10}$$

where

$$\begin{aligned}E(\theta)=&\int_{-\Lambda_x/2}^{\Lambda_x/2}\exp\left(-2\pi ix\sin\theta_x/\lambda\right)dx\\ &\times\int_{-\Lambda_y/2}^{\Lambda_y/2}T(x,y)\exp\left(-2\pi iy\sin\theta_y/\lambda\right)dy.\end{aligned} \tag{11}$$

θ_x and θ_y are the diffraction angles along the *x*- and *y*-axes with respect to the *z*-direction, respectively, and M_x and M_y are the numbers of spatial periods of the grating. The (*m*,*n*)-order diffraction angle is determined by $\sin\theta_x = m\lambda/\Lambda_x$ and $\sin\theta_y = m\lambda/\Lambda_y$.

3. Results and discussions

First, we show that it is possible to realize 2D *PT symmetry* in QWs by using 2D SW coupling and pump fields modulated in the *x*- and *y*-directions. To make a comparison, we plot the real and imaginary parts of the refractive index (n_R and n_I) in Figs. 2(a) and 2(b) for the TW coupling field ($\delta\Omega_{cx} = \delta\Omega_{cy} = 0$), respectively, and in Figs. 2(c) and 2(d) for the SW coupling field ($\delta\Omega_{cx} \neq 0, \delta\Omega_{cy} \neq 0$), respectively. Further, in two cases, the pump field is maintained as a 2D SW in both the *x*- and *y*-directions. It can be seen that when $\delta\Omega_{cx} = \delta\Omega_{cy} = 0$, n_R is asymmetric, and n_I is an even function of the lattice position *x* and *y*. In contrast, when $\delta\Omega_{cx} \neq 0, \delta\Omega_{cy} \neq 0$, n_R becomes symmetric, that is, an even function of lattice position *x* and *y*, and there is no significant change in n_I. These results clearly indicate that 2D *PT symmetry* can be built in QWs by applying 2D SW coupling and pump fields. Unlike the *PT symmetry* in atomic lattices [36], the modulation of the carrier density of QWs is not necessary. In a practical system, the ideal conditions for constructing *PT symmetry* are difficult to reach, especially in atoms or semiconductor materials. Here, we analyze the difference between $n(r)$ and $n^*(-r)$ and find that the degrees of asymmetry for n_R and n_I in Fig. 2 are below 5%, thus, it is manageable in practical systems.

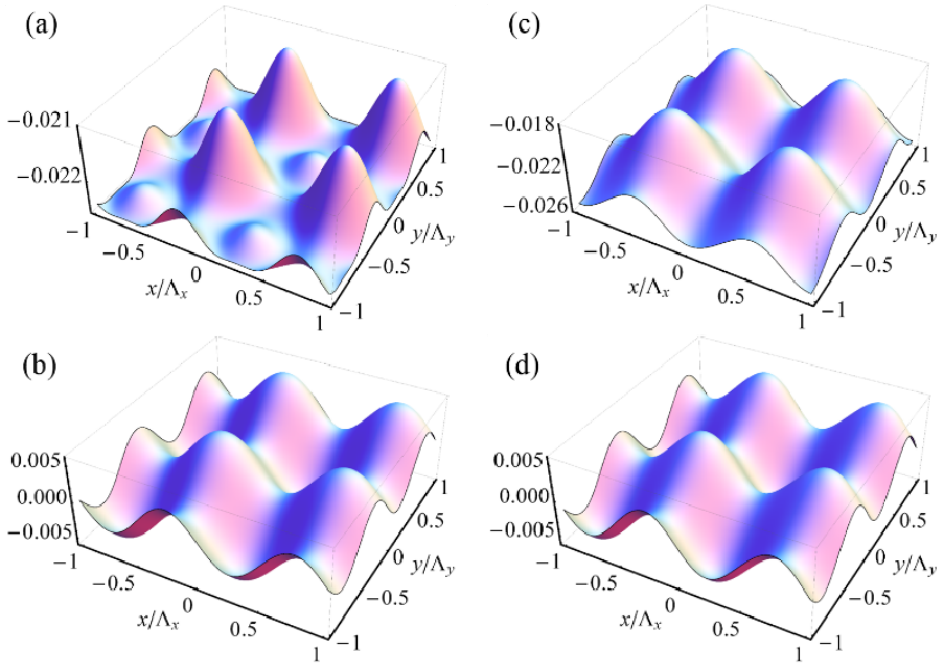

Fig. 2. (a, c) Real parts n_R and (b, d) imaginary parts n_I of the 2D complex refractive index for TW and SW coupling field, respectively. The parameters for (a) and (b) are $\delta\Omega_{cx} = \delta\Omega_{cy} = 0$ and those for (c) and (d) are $\delta\Omega_{cx} = \delta\Omega_{cy} = 0.1\text{MHz}$. The other parameters are $\Omega_p = 0.01\text{MHz}$, $\Omega_{c0} = 1\text{MHz}$, $\Omega_{d0} = 3\text{MHz}$, $\Delta_p = -3.685\text{MHz}$, $\Delta_c = \Delta_d = 0$, $\Gamma_3^{dhp} = \Gamma_3^{dhp} = 2.58\text{meV}$, $\Gamma_{3l} = \Gamma_{4l} = 2.07\text{meV}$, $M_x = M_y = 5$, $\Lambda_x/\lambda = \Lambda_y/\lambda = 4$, and $L = 500\zeta$.

Optics EXPRESS

We next consider the probe field impinging upon the QWs perpendicularly to the 2D SW (*z*-direction). Without *PT symmetry*, similar to the EIGs in previous studies, the probe field is diffracted into four domains, domain I ($0 \le \sin\theta_x, \sin\theta_y \le 1$), domain II ($-1 \le \sin\theta_x \le 0, 0 \le \sin\theta_y \le 1$), domain III ($-1 \le \sin\theta_x, \sin\theta_y \le 0$), and domain IV ($0 \le \sin\theta_x \le 1, -1 \le \sin\theta_y \le 0$), as shown in Fig. 3(a). On the contrary, with *PT symmetry*, it can be seen from Fig. 3(b) that the probe field is mainly diffracted into domain I ($0 \le \sin\theta_x, \sin\theta_y \le 1$). Therefore, by spatially manipulating the coupling field, the asymmetric light diffraction with *PT symmetry* can be constructed from symmetric light diffraction without *PT symmetry* in QW media.

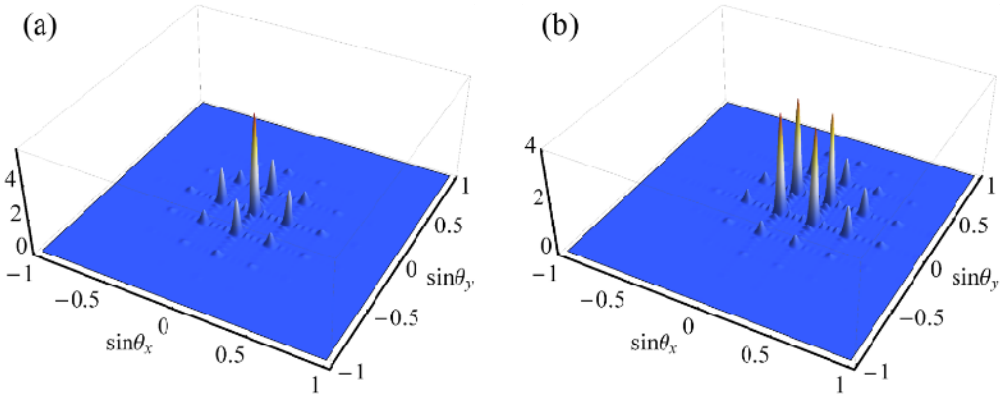

Fig. 3. (a) Diffraction intensities as a function of $(\sin\theta_x, \sin\theta_y)$ for (a) $\delta\Omega_{cx} = \delta\Omega_{cy} = 0$ and (b) $\delta\Omega_{cx} = \delta\Omega_{cy} = 0.1\text{MHz}$. The other parameters are the same as in Fig. 2.

Such asymmetric diffraction can be explained by the interference mechanism between the amplitude and phase functions of the grating. Under the condition of 2D *PT symmetry* shown in Figs. 2(c) and 2(d), the amplitude and phase functions of the grating can induce constructive interference in domain I and destructive interference in domains II, III, and IV. The constructive interference leads to the increase in the diffraction peak located in domain I, while the destructive interference leads to the decrease in the diffraction peak located in the other three domains. Therefore, asymmetric diffraction is obtained. It can be seen that the complete disappearance of the diffraction peaks in domains II, III, and IV can be realized under the condition of perfect destructive interference. It should be noted that perfect destructive interference and asymmetric diffraction can only be achieved at the exceptional point, which is determined by the ratio of n_R and n_I [37,46].

Optics EXPRESS

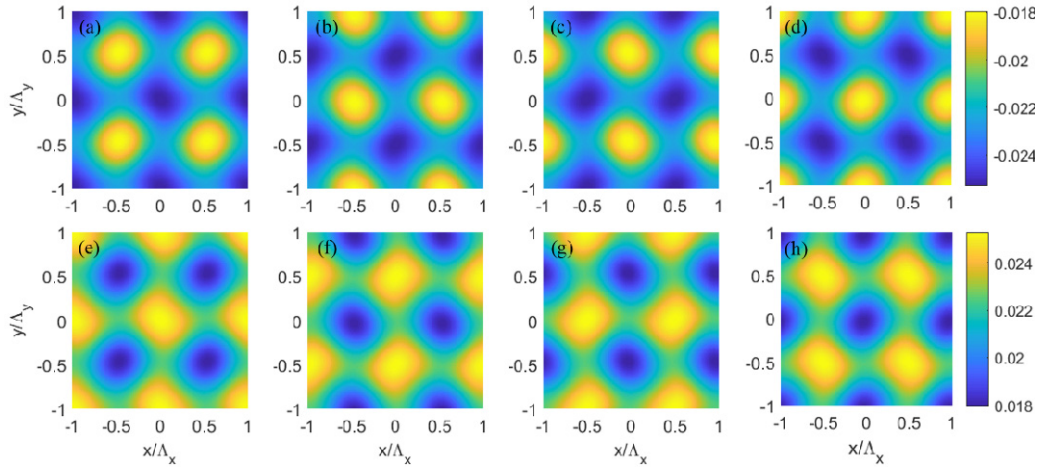

Fig. 4. Top view of the real part n_R of the 2D complex refractive index for the unchanged absolute value and different signs of Δ_p, $\delta\Omega_{cx}$ and $\delta\Omega_{cy}$, respectively; the parameters are (a) $\Delta_p = -3.685\text{MHz}$, $\delta\Omega_{cx}=0.1\text{MHz}$ and $\delta\Omega_{cy}=0.1\text{MHz}$, (b) $\Delta_p = -3.685\text{MHz}$, $\delta\Omega_{cx}=0.1\text{MHz}$ and $\delta\Omega_{cy}=-0.1\text{MHz}$, (c) $\Delta_p = -3.685\text{MHz}$, $\delta\Omega_{cx}=-0.1\text{MHz}$ and $\delta\Omega_{cy}=0.1\text{MHz}$, (d) $\Delta_p = -3.685\text{MHz}$, $\delta\Omega_{cx}=-0.1\text{MHz}$ and $\delta\Omega_{cy}=-0.1\text{MHz}$, (e) $\Delta_p = 3.685\text{MHz}$, $\delta\Omega_{cx}=0.1\text{MHz}$ and $\delta\Omega_{cy}=0.1\text{MHz}$, (f) $\Delta_p = 3.685\text{MHz}$, $\delta\Omega_{cx}=0.1\text{MHz}$ and $\delta\Omega_{cy}=-0.1\text{MHz}$, (g) $\Delta_p = 3.685\text{MHz}$, $\delta\Omega_{cx}=-0.1\text{MHz}$ and $\delta\Omega_{cy}=0.1\text{MHz}$, (h) $\Delta_p = 3.685\text{MHz}$, $\delta\Omega_{cx}=-0.1\text{MHz}$ and $\delta\Omega_{cy}=-0.1\text{MHz}$, the other parameters are the same as in Fig. 2.

Next, we will discuss the relationship between the diffraction direction of a *PT*-symmetric EIG and the spatial refractive index. The properties of the refractive index can be manipulated by varying the parameters of the laser fields. Here, we only consider changing the sign of the probe detuning Δ_p and the modulation amplitudes of the SW coupling and pump fields $\delta\Omega_{cx}$, $\delta\Omega_{cy}$, $\delta\Omega_{dx}$, and $\delta\Omega_{dy}$, because such an operation will maintain the *PT*-symmetric properties and can be easily realized in the experiment. We calculate all kinds of spatial refractive indices under different combinations of these five parameters, finding that the sign of Δ_p, $\delta\Omega_{cx}$ and $\delta\Omega_{cy}$ results in different n_R and has little effect on n_I, while the sign of $\delta\Omega_{dx}$ and $\delta\Omega_{dy}$ results in different n_I and has little effect on n_R. We plot n_R for different sign of Δ_p, $\delta\Omega_{cx}$ and $\delta\Omega_{cy}$ in Fig. 4 (2^3 kinds of combinations), and n_I for different sign of $\delta\Omega_{dx}$ and $\delta\Omega_{dy}$ in Fig. 5 (2^2 kinds of combinations), respectively. Therefore, there are total $2^3 \times 2^2$ kinds of spatial refractive indices, which are all *PT symmetry* and have different spatial properties.

Optics EXPRESS

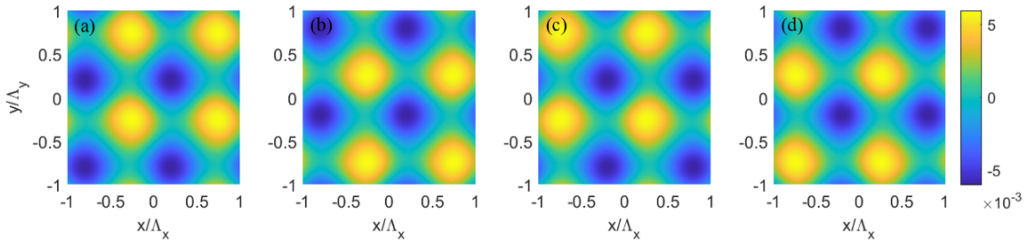

Fig. 5. Top view of the imaginary part n_I of the 2D complex refractive index for the unchanged absolute value and different signs of $\delta\Omega_{dx}$ and $\delta\Omega_{dy}$, respectively; the parameters are (a) $\delta\Omega_{dx}=0.1\text{MHz}$ and $\delta\Omega_{dy}=0.1\text{MHz}$, (b) $\delta\Omega_{dx}=0.1\text{MHz}$ and $\delta\Omega_{dy}=-0.1\text{MHz}$, (c) $\delta\Omega_{dx}=-0.1\text{MHz}$ and $\delta\Omega_{dy}=0.1\text{MHz}$, (d) $\delta\Omega_{dx}=-0.1\text{MHz}$ and $\delta\Omega_{dy}=-0.1\text{MHz}$. The other parameters are the same as in Fig. 2.

These different kinds of spatial refractive indices will result in asymmetric light diffraction in the four different domains (Fig. 6). For instance, under eight kinds of spatial refractive indices (Table 1), the amplitude and phase functions of the grating can induce constructive interference in domain I and destructive interference in domains II, III, and IV, thus, the probe field will mainly be diffracted into domain I [Fig. 6(b)]. Other spatial refractive indices will resulting in the asymmetric diffraction in other domains.

Table 1. Different signs of Δ_p, $\delta\Omega_{cx}$, $\delta\Omega_{cy}$, $\delta\Omega_{dx}$, and $\delta\Omega_{dy}$.

	Δ_p	$\delta\Omega_{cx}$	$\delta\Omega_{cy}$	n_R	$\delta\Omega_{dx}$	$\delta\Omega_{dy}$	n_I
1	–	+	+	Figure 4(a)	+	+	Figure 5(a)
2	–	+	+	Figure 4(a)	–	–	Figure 5(d)
3	–	–	–	Figure 4(d)	+	+	Figure 5(a)
4	–	–	–	Figure 4(d)	–	–	Figure 5(d)
5	+	+	–	Figure 4(f)	+	–	Figure 5(b)
6	+	–	+	Figure 4(g)	+	–	Figure 5(b)
7	+	+	–	Figure 4(f)	–	+	Figure 5(c)
8	+	–	+	Figure 4(g)	–	+	Figure 5(c)

Optics EXPRESS

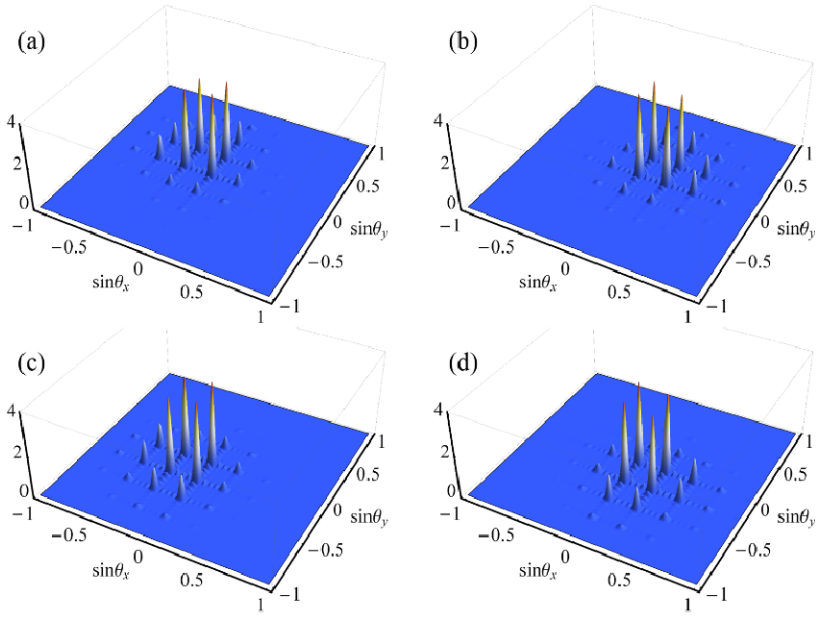

Fig. 6. Diffraction patterns with *PT symmetry* as a function of ($\sin\theta_x, \sin\theta_y$) in different domains: (a) domain I ($0 \le \sin\theta_x, \sin\theta_y \le 1$), (b) domain II ($-1 \le \sin\theta_x \le 0, 0 \le \sin\theta_y \le 1$), (c) domain III ($-1 \le \sin\theta_x, \sin\theta_y \le 0$), and (d) domain IV ($0 \le \sin\theta_x \le 1, -1 \le \sin\theta_y \le 0$).

Furthermore, the direction of the probe field (along + *z*-direction with wave vector k_z or – *z*-direction with wave vector $-k_z$) will not affect the diffraction direction of a *PT*-symmetric EIG. When the probe field with wave vector k_z or $-k_z$ propagates through the spatially modulated grating (*x*–*y* plane), it will also exhibit wave vectors ± k_x and ± k_y. With the *PT symmetry* shown in Figs. 2(c) and 2(d), only the selected components of + k_x and + k_y will be reflected at the ends of the grating; therefore, the photons will be diffracted only to the selected domain, domain I ($0 \le \sin\theta_x, \sin\theta_y \le 1$). The spatial modulation of the complex refractive index in the *x*–*y* plane remains the same under the condition of unchanged spatial distributions of the coupling and pump fields. Thus, the diffracted photons are biased toward domain I regardless of whether the probe field propagates along the + *z*-direction or –*z*-direction.

Finally, we consider the intensity distribution of the diffraction depending on the interaction length ζ. As can be seen in Fig. 7(a), when ζ is small, most of the energy is distributed in the (0,0)-order diffraction peak. As ζ increases, because of the enhanced phase modulation depth, the energy is gradually transferred to the higher-order diffraction peak in domain I ($0 \le \sin\theta_x, \sin\theta_y \le 1$), as shown in Figs. 7(b) and 7(c). With a further increase in ζ, more energy is transferred to the high-order diffraction peaks, and the highest diffraction peak is the (1,1)-order diffraction peak, which is located in the direction determined by $\sin\theta_x = \sin\theta_y = 0.25$ [Fig. 7(d)]. Thus, one can control the intensity distribution of the diffraction by adjusting the interaction length ζ when the probe field passes through a QW system.

Optics EXPRESS

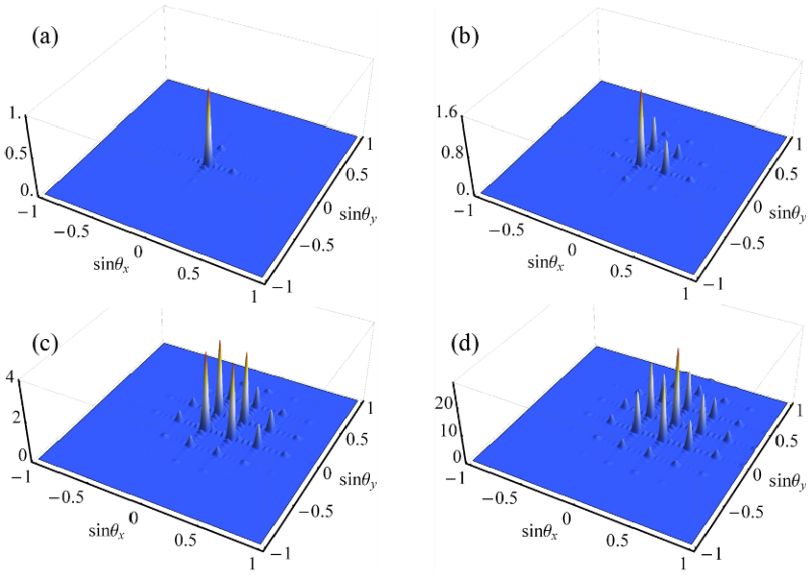

Fig. 7. Diffraction intensities with *PT symmetry* as a function of ($\sin\theta_x$, $\sin\theta_y$) for different values of the interaction length: (a) $L=100\zeta$, (b) $L=300\zeta$, (c) $L=500\zeta$, and (d) $L=700\zeta$. The other parameters are the same as in Fig. 2.

4. Conclusions

In summary, we have demonstrated that 2D *PT symmetry* and a 2D EIG can be realized in an asymmetric double semiconductor QW driven by one TW probe field and 2D SW coupling and pump fields. We have demonstrated that the incident probe field traveling through such a *PT symmetry* grating can be diffracted to the selected domain, which results from the interference mechanism between the amplitude and phase of the grating. We have found that such asymmetric diffraction patterns are determined by the spatial relationship of the real and imaginary parts of the refractive index and can be controlled by the sign of the probe field and the modulation amplitudes of the 2D SW coupling and pump fields. We have also found that the intensity distribution in the selected angles can be manipulated by varying the interaction length of the medium. Such a QW system can provide a versatile platform for theoretically and experimentally exploring *PT*-symmetric phenomena and can be used to develop new photoelectric devices requiring asymmetric light transport using semiconductor materials.

Funding

National Natural Science Foundation of China (NSFC) (61774156, 61761136009); External Cooperation Program of the Chinese Academy of Sciences (181722KYSB20160005); Jilin Provincial Natural Science Foundation (20160520095JH, 20180519024JH); The Program of China Scholarships Council (201604910385); Youth Innovation Promotion Association of the Chinese Academy of Sciences (2018249).

References

1. M. Fleischhauer, A. Imamoglu, and J. P. Marangos, "Electromagnetically induced transparency: Optics in coherent media," Rev. Mod. Phys. **77**(2), 633–673 (2005).
2. S. E. Harris, "Electromagnetically induced transparency," Phys. Today **50**(7), 36–42 (1997).
3. J. P. Marangos, "Electromagnetically induced transparency," J. Mod. Opt. **45**(3), 471–503 (1998).
4. L. V. Hau, S. E. Harris, Z. Dutton, and C. H. Behroozi, "Light speed reduction to 17 metres per second in an ultracold atomic gas," Nature **397**(6720), 594–598 (1999).
5. A. V. Turukhin, V. S. Sudarshanam, M. S. Shahriar, J. A. Musser, B. S. Ham, and P. R. Hemmer, "Observation of ultraslow and stored light pulses in a solid," Phys. Rev. Lett. **88**(2), 023602 (2001).

Optics EXPRESS

6. C. Liu, Z. Dutton, C. H. Behroozi, and L. V. Hau, "Observation of coherent optical information storage in an atomic medium using halted light pulses," Nature **409**(6819), 490–493 (2001).
7. D. F. Phillips, A. Fleischhauer, A. Mair, R. L. Walsworth, and M. D. Lukin, "Storage of light in atomic vapor," Phys. Rev. Lett. **86**(5), 783–786 (2001).
8. S. E. Harris and Y. Yamamoto, "Photon switching by quantum interference," Phys. Rev. Lett. **81**(17), 3611–3614 (1998).
9. M. Yan, E. G. Rickey, and Y. Zhu, "Observation of absorptive photon switching by quantum interference," Phys. Rev. A **64**(4), 041801 (2001).
10. H. Schmidt and A. Imamoglu, "Giant Kerr nonlinearities obtained by electromagnetically induced transparency," Opt. Lett. **21**(23), 1936–1938 (1996).
11. H. Wang, D. Goorskey, and M. Xiao, "Enhanced Kerr nonlinearity via atomic coherence in a three-level atomic system," Phys. Rev. Lett. **87**(7), 073601 (2001).
12. Y. Wu, L. Wen, and Y. Zhu, "Efficient hyper-Raman scattering in resonant coherent media," Opt. Lett. **28**(8), 631–633 (2003).
13. Y. Zhang, A. W. Brown, and M. Xiao, "Observation of interference between four-wave mixing and six-wave mixing," Opt. Lett. **32**(9), 1120–1122 (2007).
14. A. André and M. D. Lukin, "Manipulating light pulses via dynamically controlled photonic band gap," Phys. Rev. Lett. **89**(14), 143602 (2002).
15. M. Artoni and G. C. La Rocca, "Optically tunable photonic stop bands in homogeneous absorbing media," Phys. Rev. Lett. **96**(7), 073905 (2006).
16. H. Y. Ling, Y.-Q. Li, and M. Xiao, "Electromagnetically induced grating: Homogeneously broadened medium," Phys. Rev. A **57**(2), 1338–1344 (1998).
17. M. Mitsunaga and N. Imoto, "Observation of an electromagnetically induced grating in cold sodium atoms," Phys. Rev. A **59**(6), 4773–4776 (1999).
18. G. C. Cardoso and J. W. R. Tabosa, "Electromagnetically induced gratings in a degenerate open two-level system," Phys. Rev. A **65**(3), 033803 (2002).
19. L. E. E. de Araujo, "Electromagnetically induced phase grating," Opt. Lett. **35**(7), 977–979 (2010).
20. R.-G. Wan, J. Kou, L. Jiang, Y. Jiang, and J.-Y. Gao, "Electromagnetically induced grating via enhanced nonlinear modulation by spontaneously generated coherence," Phys. Rev. A **83**(3), 033824 (2011).
21. A. W. Brown and M. Xiao, "All-optical switching and routing based on an electromagnetically induced absorption grating," Opt. Lett. **30**(7), 699–701 (2005).
22. Y. Zhang, Z. Wang, Z. Nie, C. Li, H. Chen, K. Lu, and M. Xiao, "Four-wave mixing dipole soliton in laser-induced atomic gratings," Phys. Rev. Lett. **106**(9), 093904 (2011).
23. Y. Zhang, Z. Wu, M. R. Belić, H. Zheng, Z. Wang, M. Xiao, and Y. Zhang, "Photonic Floquet topological insulators in atomic ensembles," Laser Photonics Rev. **9**(3), 331–338 (2015).
24. C. M. Bender and S. Boettcher, "Real spectra in non-Hermitian Hamiltonians having PT symmetry," Phys. Rev. Lett. **80**(24), 5243–5246 (1998).
25. R. El-Ganainy, K. G. Makris, D. N. Christodoulides, and Z. H. Musslimani, "Theory of coupled optical PT-symmetric structures," Opt. Lett. **32**(17), 2632–2634 (2007).
26. A. Guo, G. J. Salamo, D. Duchesne, R. Morandotti, M. Volatier-Ravat, V. Aimez, G. A. Siviloglou, and D. N. Christodoulides, "Observation of PT-symmetry breaking in complex optical potentials," Phys. Rev. Lett. **103**(9), 093902 (2009).
27. C. E. Rüter, K. G. Makris, R. El-Ganainy, D. N. Christodoulides, M. Segev, and D. Kip, "Observation of parity-time symmetry in optics," Nat. Phys. **6**(3), 192–195 (2010).
28. Z. H. Musslimani, K. G. Makris, R. El-Ganainy, and D. N. Christodoulides, "Optical solitons in PT periodic potentials," Phys. Rev. Lett. **100**(3), 030402 (2008).
29. S. Longhi, "Bloch oscillations in complex crystals with PT Symmetry," Phys. Rev. Lett. **103**(12), 123601 (2009).
30. H. Ramezani, T. Kottos, R. El-Ganainy, and D. N. Christodoulides, "Unidirectional nonlinear PT-symmetric optical structures," Phys. Rev. A **82**(4), 043803 (2010).
31. Z. Lin, H. Ramezani, T. Eichelkraut, T. Kottos, H. Cao, and D. N. Christodoulides, "Unidirectional Invisibility Induced by PT-Symmetric Periodic Structures," Phys. Rev. Lett. **106**(21), 213901 (2011).
32. L. Feng, Y.-L. Xu, W. S. Fegadolli, M.-H. Lu, J. E. B. Oliveira, V. R. Almeida, Y.-F. Chen, and A. Scherer, "Experimental demonstration of a unidirectional reflectionless parity-time metamaterial at optical frequencies," Nat. Mater. **12**(2), 108–113 (2013).
33. L. Chang, X. Jiang, S. Hua, C. Yang, J. Wen, L. Jiang, G. Li, G. Wang, and M. Xiao, "Parity-time symmetry and variable optical isolation in active-passive-coupled microresonators," Nat. Photonics **8**(7), 524–529 (2014).
34. B. Peng, S. K. Ozdemir, F. Lei, F. Monifi, M. Gianfreda, G. L. Long, S. Fan, F. Nori, C. M. Bender, and L. Yang, "Parity-time-symmetric whispering-gallery microcavities," Nat. Phys. **10**(5), 394–398 (2014).
35. M. Kulishov, J. Laniel, N. Bélanger, J. Azaña, and D. Plant, "Nonreciprocal waveguide Bragg gratings," Opt. Express **13**(8), 3068–3078 (2005).
36. Y.-M. Liu, F. Gao, C.-H. Fan, and J.-H. Wu, "Asymmetric light diffraction of an atomic grating with PT symmetry," Opt. Lett. **42**(21), 4283–4286 (2017).
37. T. Shui, W.-X. Yang, S. Liu, L. Li, and Z. Zhu, "Asymmetric diffraction by atomic gratings with optical PT symmetry in the Raman-Nath regime," Phys. Rev. A (Coll. Park) **97**(3), 033819 (2018).

Optics EXPRESS

38. Y. D. Chong, L. Ge, H. Cao, and A. D. Stone, "Coherent perfect absorbers: time-reversed lasers," Phys. Rev. Lett. **105**(5), 053901 (2010).
39. S. Longhi, "PT-symmetric laser absorber," Phys. Rev. A **82**(3), 031801 (2010).
40. L. Feng, Z. J. Wong, R.-M. Ma, Y. Wang, and X. Zhang, "Single-mode laser by parity-time symmetry breaking," Science **346**(6212), 972–975 (2014).
41. H. Hodaei, M.-A. Miri, M. Heinrich, D. N. Christodoulides, and M. Khajavikhan, "Parity-time-symmetric microring lasers," Science **346**(6212), 975–978 (2014).
42. H. Jing, S. K. Özdemir, X.-Y. Lü, J. Zhang, L. Yang, and F. Nori, "PT-symmetric phonon laser," Phys. Rev. Lett. **113**(5), 053604 (2014).
43. B. He, L. Yang, and M. Xiao, "Dynamical phonon laser in coupled active-passive microresonators," Phys. Rev. A (Coll. Park) **94**(3), 031802 (2016).
44. C. Hang, G. Huang, and V. V. Konotop, "PT Symmetry with a system of three-level atoms," Phys. Rev. Lett. **110**(8), 083604 (2013).
45. H. J. Li, J. P. Dou, and G. Huang, "PT symmetry via electromagnetically induced transparency," Opt. Express **21**(26), 32053–32062 (2013).
46. J. Sheng, M.-A. Miri, D. N. Christodoulides, and M. Xiao, "PT-symmetric optical potentials in a coherent atomic medium," Phys. Rev. A **88**(4), 041803 (2013).
47. Z. Zhang, Y. Zhang, J. Sheng, L. Yang, M.-A. Miri, D. N. Christodoulides, B. He, Y. Zhang, and M. Xiao, "Observation of Parity-Time Symmetry in optically induced atomic lattices," Phys. Rev. Lett. **117**(12), 123601 (2016).
48. G. B. Serapiglia, E. Paspalakis, C. Sirtori, K. L. Vodopyanov, and C. C. Phillips, "Laser-induced quantum coherence in a semiconductor quantum well," Phys. Rev. Lett. **84**(5), 1019–1022 (2000).
49. M. Phillips and H. Wang, "Electromagnetically induced transparency due to intervalence band coherence in a GaAs quantum well," Opt. Lett. **28**(10), 831–833 (2003).
50. J. F. Dynes, M. D. Frogley, M. Beck, J. Faist, and C. C. Phillips, "AC Stark splitting and quantum interference with intersubband transitions in quantum wells," Phys. Rev. Lett. **94**(15), 157403 (2005).
51. M. D. Frogley, J. F. Dynes, M. Beck, J. Faist, and C. C. Phillips, "Gain without inversion in semiconductor nanostructures," Nat. Mater. **5**(3), 175–178 (2006).
52. J.-H. Wu, J.-Y. Gao, J.-H. Xu, L. Silvestri, M. Artoni, G. C. La Rocca, and F. Bassani, "Ultrafast all optical switching via tunable Fano interference," Phys. Rev. Lett. **95**(5), 057401 (2005).
53. H. G. Roskos, M. C. Nuss, J. Shah, K. Leo, D. A. B. Miller, A. M. Fox, S. Schmitt-Rink, and K. Köhler, "Coherent submillimeter-wave emission from charge oscillations in a double-well potential," Phys. Rev. Lett. **68**(14), 2216–2219 (1992).
54. W.-X. Yang and R.-K. Lee, "Controllable entanglement and polarization phase gate in coupled double quantum-well structures," Opt. Express **16**(22), 17161–17170 (2008).
55. C. Zhu and G. Huang, "Slow-light solitons in coupled asymmetric quantum wells via interband transitions," Phys. Rev. B Condens. Matter Mater. Phys. **80**(23), 235408 (2009).
56. X. Q. Luo, D. L. Wang, Z. Q. Zhang, J. W. Ding, and W. M. Liu, "Nonlinear optical behavior of a four-level quantum well with coupled relaxation of optical and longitudinal phonons," Phys. Rev. A **84**(3), 033803 (2011).
57. D. E. Nikonov, A. Imamoğlu, L. V. Butov, and H. Schmidt, "Collective intersubband excitations in quantum wells: coulomb interaction versus subband dispersion," Phys. Rev. Lett. **79**(23), 4633–4636 (1997).
58. Y. Y. Chen, Z. Z. Liu, and R. G. Wan, "Two-dimensional electromagnetically induced grating in coherent atomic medium," Europhys. Lett. **116**(6), 64006 (2016).